Optimizing Continuity in Multiscale Imagery

Charles Han
Columbia University

Hugues Hoppe
Microsoft Research

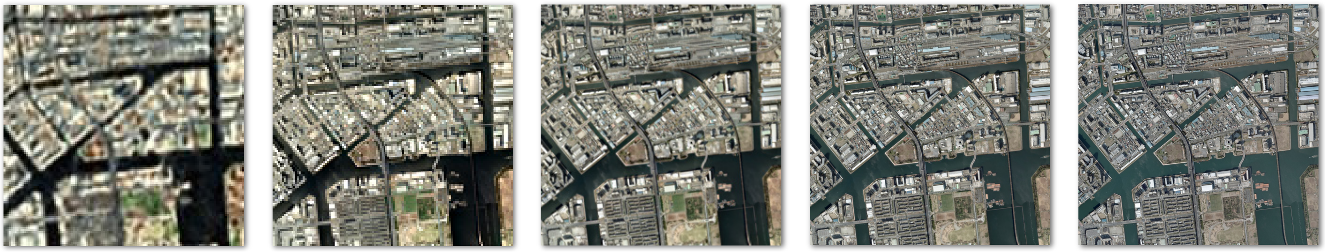

(a) Input coarse image (128^2 resolution)
(b) New coarse image with structure transf. from (e)
(c) Solved intermediate level (256^2)
(d) Solved intermediate level (512^2)
(e) Input fine image (1024^2)

Figure 1: *Given both coarse and fine imagery (a,e), we construct a mipmap image pyramid with smooth visual transitions across scales. Our approach uses two new techniques: (b) structure transfer, which combines fine-scale detail and coarse-scale appearance to reduce ghosting artifacts, and (c,d) clipped Laplacian blending, which creates the intermediate resolution levels so as to avoid blurring.*

Abstract

Multiscale imagery often combines several sources with differing appearance. For instance, Internet-based maps contain satellite and aerial photography. Zooming within these maps may reveal jarring transitions. We present a scheme that creates a visually smooth mipmap pyramid from stitched imagery at several scales. The scheme involves two new techniques. The first, *structure transfer*, is a nonlinear operator that combines the detail of one image with the local appearance of another. We use this operator to inject detail from the fine image into the coarse one while retaining color consistency. The improved structural similarity greatly reduces inter-level ghosting artifacts. The second, *clipped Laplacian blending*, is an efficient construction to minimize blur when creating intermediate levels. It considers the sum of all inter-level image differences within the pyramid. We demonstrate continuous zooming of map imagery from space to ground level.

Keywords: mipmap pyramid, structure transfer.

1 Introduction

There is a large body of work in the computer graphics and GIS communities on stitching and fusing collections of images to form seamless maps or panoramas (Section 2). Such techniques have been used to assemble the large datasets available on Internet services like Keyhole, TerraServer, Bing Maps, Google Maps, and Yahoo Maps.

These multiresolution datasets incorporate several sources of imagery at different scales – for instance, satellite at coarse resolution and aerial photography at fine scale. The data sources often vary significantly in appearance due to differences in spectral response, seasonal changes, lighting and shadows, and custom image processing. Therefore, zooming within the multiresolution image pyramid often results in abrupt changes in appearance, i.e., temporal "popping". In addition, spatial discontinuities may be observed in static perspective views, as these access several mipmap levels simultaneously (Figure 3).

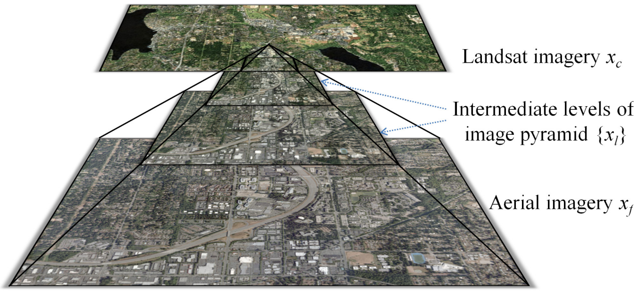

Figure 2: *Given sparsely defined fine-scale imagery, we create an image pyramid that is continuous across scales yet preserves the appearance uniformity of the coarse-scale image.*

Goal We create a visually smooth image pyramid that combines different data sources at different scales (Figures 1 and 2). The input imagery is given at a subset of levels, and is assumed to be already stitched spatially using existing techniques. While the problem of creating a full image pyramid may seem simple, several straightforward approaches have drawbacks:

- One idea is to downsample the fine imagery all the way to the coarsest level of the pyramid, overwriting any coarser image content. However, fine-scale imagery is often sparsely defined, and therefore the resulting coarser levels may have nonuniform appearance (Figure 4). Instead, we want to preserve the spatial consistency of the coarse-scale image.
- Another idea is to modify the fine-scale imagery to have the same color appearance as the coarse-scale content. However, it is desirable to have distinct color histograms at coarse and fine scales. Particularly, satellite imagery is often artificially colored to achieve an exaggerated appearance; it would be undesirable to apply this abstract coloring to aerial photography, which typically has a richer, more natural color histogram.

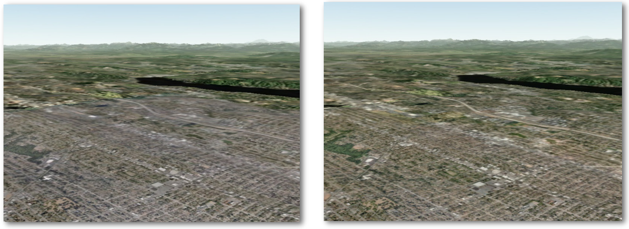

(a) Original image pyramid (b) Result of our scheme

Figure 3: *Appearance differences across image pyramid levels are noticeable in perspective views. (Example from Bing Maps.)*

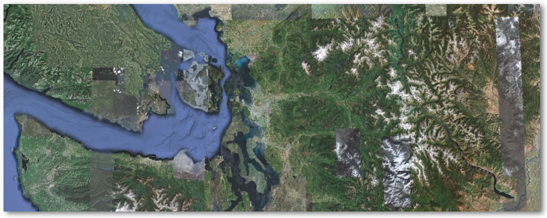

Figure 4: *Replacing coarse pyramid levels by downsampling the sparse fine imagery may lead to a patchwork appearance at coarser levels. (Example from Google Earth.)*

Our aim is to simultaneously satisfy both multiresolution and spatial continuity. These two objectives can be expressed as:

(1) minimizing visual differences between all adjacent levels of the image pyramid, while

(2) preserving the color characteristics of both the coarse-scale and fine-scale imagery.

The visual difference between two images is often measured using the mean squared error (MSE) of corresponding pixels. While this simple pointwise metric leads to convenient linear systems, it does not accurately capture the perceptual characteristics of the human visual system. Rather, a metric that emphasizes *structural similarity* (SSIM) has been shown to be much more effective [Wang et al. 2004], and we adopt it in our approach.

In particular, we will show that minimizing MSE alone results in an image pyramid with severe ghosting artifacts. The fundamental problem is that the coarse and fine images have differences in structural detail due to misregistration, parallax, or many other factors in image acquisition and processing. Explicitly considering structural similarity helps to overcome ghosting.

Scheme Maximizing structural similarity is unfortunately a nonlinear problem, and therefore expensive to solve directly. To attain an efficient solution, we divide the problem into two simpler parts (see Figure 5):

(1) To maximize structural compatibility, we develop a *structure transfer* operation. It modifies the coarse image to inherit the detail of the fine image while preserving its original local color characteristics (Section 5).

(2) Given the now structurally compatible images, we minimize the sum of all inter-level image differences within the pyramid using the simple MSE metric. An important detail is that this difference functional must be defined judiciously to avoid signal blurring. Although minimizing MSE is a linear problem, a global solution over all pixels in a large pyramid is still costly. We show that a good approximate solution can be found using an efficient construction, *clipped Laplacian blending* (Section 6).

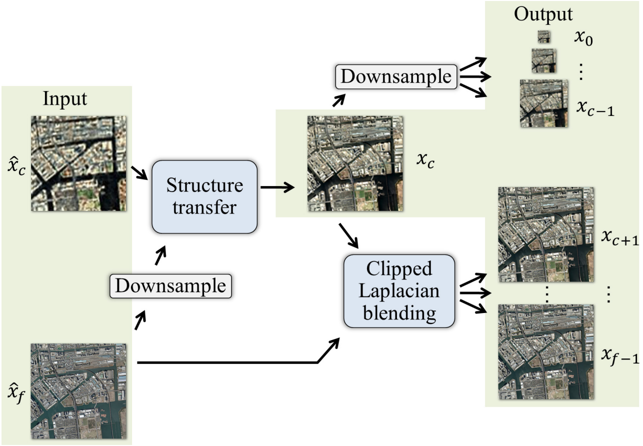

Figure 5: *Schematic overview of our algorithm.*

The overall process is illustrated in Figure 5. Structure transfer combines the coarse image with the downsampled version of the fine image. Next, clipped Laplacian blending creates the intermediate levels. Finally, the structure-transferred coarse image is downsampled so that its new detail structure is propagated to even coarser levels. The improvements in multiscale continuity due to our two novel techniques are demonstrated in Figure 6.

The image pyramid construction is performed entirely as a preprocess, so any 2D or 3D client renderer need not be modified to benefit from the improved multiresolution continuity.

2 Related work

Image stitching and fusion Merging overlapping images to form a seamless composite is an active area in computer graphics [e.g., Pérez et al. 2003; Agarwala et al. 2004; Szeliski 2006]. There is also significant work on fusion techniques that combine information from different types of sensors into a single image [Stathaki 2008]. In particular, several techniques merge low-resolution multispectral and high-resolution grayscale images [e.g. Chavez et al. 1991; Pohl and Van Genderen 1998]. Our work assumes that different content sources have already been stitched or fused at two or more scales, and aims to create a complete pyramid that spans these stitched source images.

Image pyramids Multiscale structures are commonly used to represent, analyze, and process a given image. A mipmap pyramid provides a prefiltered representation for antialiased texture mapping [Williams 1983]. Laplacian image pyramids [Burt and Adelson 1983a], scale-space representations [Witkin 1983], and image wavelets [Antonini et al. 1992] allow efficient processing of bandpass data that is localized in both frequency and spatial domains. Multiscale representations are used to merge images given at the same scale [Burt and Adelson 1983b]. To our knowledge, there is little work on creating a continuous pyramid from images provided at different scales.

Image transfer Reinhard et al. [2001] transfer appearance from one image to another using global color statistics. Their operator can be seen as a global analogue to our localized structure transfer (Section 5). Whereas their technique operates on two arbitrary images, ours is tailored for identical views of the same scene under differing appearance. Liu et al. [2001] transfer detail from one face to another while preserving illumination using ratio images. Kopf et al. [2007] introduce the joint-bilateral upsampling filter, which allows operations performed on a downsampled image to be transferred to the original image.

Image histogram manipulation Windowed histogram equalization achieves adaptive contrast enhancement by normalizing the histogram within local windows of the image [Pizer et al. 1987]. Histogram-transfer modifies one image to adopt the global color histogram of another image [Gonzalez and Woods 1992; Pitié et al. 2007]. Our structure transfer operation builds on these ideas; it transfers local color distributions using a window-based approach.

Other related work Pang et al. [2008] apply the SSIM metric to structure-aware half-toning. Oliva et al. [2006] present hybrid images, which superimpose features from two images to create a single image that is perceived differently at two different scales.

3 Preliminaries

We denote an image pyramid by a set $\mathcal{X} = \{x_0, \ldots, x_f\}$ where the coarsest image x_0 contains a single pixel, and each image x_l has $2^l \times 2^l$ pixels. The most common form is a Gaussian pyramid, in which each level contains a low-pass filtered version of a given fine image x_f. Denoted by $\mathcal{G}$, it is formed by successively applying a *downsampling* filter:

$$\mathcal{G}_f = x_f, \quad \mathcal{G}_{l-1} = D_l \mathcal{G}_l,$$

where the rows of the sparse matrix D_l encode the filter weights.

Another useful form is a Laplacian or bandpass pyramid, which contains differences between successive Gaussian levels. More precisely, each Laplacian level contains the difference between the current Gaussian level and an *upsampled* version of the next-coarser Gaussian level:

$$\mathcal{L}_0 = \mathcal{G}_0, \quad \mathcal{L}_l = \mathcal{G}_l - U_{l-1}\mathcal{G}_{l-1}.$$

We define the upsampling matrix U, using the bicubic filter of Keys [1981], which is also known as Catmull-Rom interpolation. It is a tensor product of two 1D filters. Evaluated on the pyramid, each 1D filter has weights $(-9\ 111\ 29\ -3)/128$ and $(-3\ 29\ 111\ -9)/128$ on alternate pixels.

The downsampling filter is selected by taking the transpose of the upsampling matrix, i.e., $D_l = U_{l-1}^T$. Consequently its 1D weights are $(-3\ -9\ 29\ 111\ 111\ 29\ -9\ -3)/256$. It yields much better results than a simple box filter with weights $(1\ 1)/2$. Let $U_k^l = U_k U_{k+1} \cdots U_{l-1}$ denote the product of upsampling matrices from coarser level k to finer level l, and similarly for the downsampling matrix D_l^k.

We perform all computations in the CIE Lab color space, which is more perceptually faithful than RGB space.

4 Our approach

The inputs to our algorithm are coarse and fine images $\hat{x}_c$ and $\hat{x}_f$, respectively, and our output will be image pyramid levels $\{x_l\}$. The finest level $x_f = \hat{x}_f$ will remain unmodified. We begin by defining a quantitative objective both to guide the design of our algorithm and to evaluate results. Because explicitly maximizing the objective is costly, we will develop a practical algorithm that efficiently approximates it.

Objective functional Our goal is to minimize visual differences between successive pyramid levels, while preserving the color characteristics of the coarser pyramid levels. We formulate these two goals as the maximization of the objective

$$E(\mathcal{X}) = \sum_{l=1 \ldots f-1} \mathrm{MSSIM}(D_l x_l, x_{l-1}) + \sum_{l=0 \ldots c} \mathrm{Mlc}(x_l, D_c^l \hat{x}_c). \quad (1)$$

The first term sums the mean structural similarity (MSSIM) of all adjacent pyramid levels. As detailed in [Wang et al. 2004], $\mathrm{MSSIM}(x, y)$ of two images x, y is the mean SSIM over all corresponding 11×11 pixel neighborhoods $u \subset x, v \subset y$. The neighborhood SSIM is defined as the product of 3 factors:

$$\mathrm{SSIM}(u, v) = l(u, v) \cdot c(u, v) \cdot s(u, v).$$

The *luminance* similarity l, the *contrast* similarity c, and the *structure* comparison s are defined in terms of the mean colors μ, standard deviations σ, and covariance σ_{uv} of the neighborhoods:

$$l(u, v) = \frac{2\mu_u\mu_v + c_1}{\mu_u^2 + \mu_v^2 + c_1}, \quad c(u, v) = \frac{2\sigma_u\sigma_v + c_2}{\sigma_u^2 + \sigma_v^2 + c_2}, \quad s(u, v) = \frac{\sigma_{uv} + c_3}{\sigma_u\sigma_v + c_3}.$$

These neighborhood statistics are weighted with a spatial Gaussian kernel with a standard deviation of 2 pixels. The small constants c_1, c_2, c_3 exist to ensure numerical stability, and are set as in [Wang et al. 2004]. The product above simplifies to

$$\mathrm{SSIM}(u, v) = \frac{(2\mu_u\mu_y + c_1)(2\sigma_{uv} + c_2)}{(\mu_u^2 + \mu_v^2 + c_1)(\sigma_u^2 + \sigma_v^2 + c_2)}.$$

We compute SSIM over each color channel independently and take their mean. The MSSIM measure reaches a maximum value of 1.0 when two images are identical.

The second term of (1) measures the color similarity of the original and modified coarse image levels. Specifically, the mean luminance-contrast similarity keeps only the first two factors:

$$\mathrm{Mlc}(x, y) = \tfrac{1}{|x|} \textstyle\sum_{u \subset x, v \subset y} l(u, v) \cdot c(u, v),$$

and thus ignores structural detail. Because the finer image x_f is unaltered in our construction, it is unnecessary to measure its color fidelity.

Algorithm Maximizing $E(\mathcal{X})$ is a nonlinear problem over many variables, and is therefore difficult to directly optimize. Instead, we approximate this maximization using a three-step approach:

- Step 1: Replace $\hat{x}_c$ by x_c to maximize

$$\max_{x_c} \ \mathrm{Ms}(x_c, D_f^c x_f) + \mathrm{Mlc}(x_c, \hat{x}_c), \quad (2)$$

where the first term measures only structural compatibility:

$$\mathrm{Ms}(x, y) = \tfrac{1}{|x|} \textstyle\sum_{u \subset x, v \subset y} s(u, v).$$

This first step finds a new coarse image that is structurally similar to the downsampled fine image but whose color characteristics match those of the input coarse image $\hat{x}_c$. Structure transfer is a fast local algorithm that approximates this (Section 5).

- Step 2: Create the intermediate image levels as

$$\min_{x_{c+1} \cdots x_{f-1}} \sum_{l=c..f-1} 4^{-l} \|D_{l+1} x_{l+1} - x_l\|^2, \quad (3)$$

which minimizes the mean-squared error between each pyramid level and the downsampled next-finer level. Intuitively, the structural compatibility provided by Step 1 allows us to construct the intermediate images using this simple (linear) MSE metric in place of the more complicated MSSIM term of Equation (1). Furthermore, our clipped Laplacian blending provides a fast approximate solution to this optimization (Section 6).

- Step 3: Replace the coarser levels by downsampling x_c.

This downsampling makes all coarser levels structurally identical (i.e., $\mathrm{MSSIM}(D_l x_l, x_{l-1}) = 1$ for $l \leq c$). Because we maximize $\mathrm{Mlc}(x_c, \hat{x}_c)$ in Step 1 and downsampling preserves luminance and contrast, $\mathrm{Mlc}(x_l, D_c^l \hat{x}_c)$ is also high for coarser levels $l < c$.

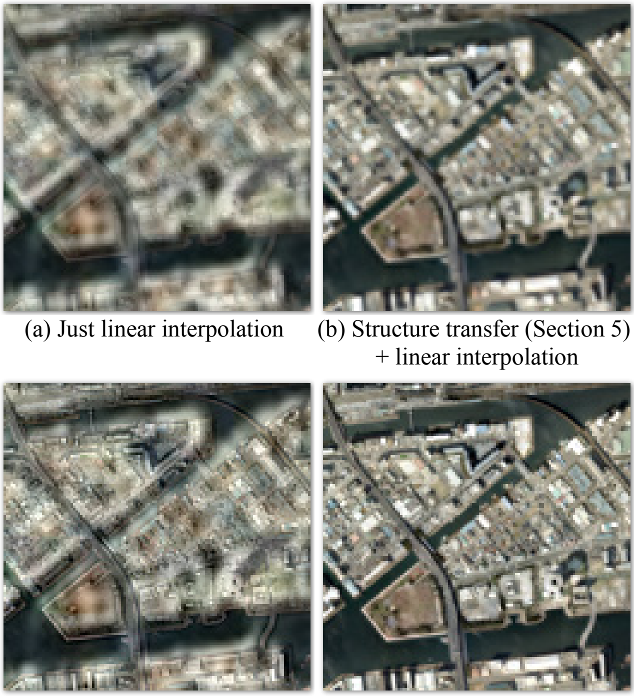

(a) Just linear interpolation

(b) Structure transfer (Section 5) + linear interpolation

(c) Just CLB (Section 6)

(d) Structure transfer + CLB

Figure 6: *Close-ups comparing the blended images at 256^2 resolution obtained with different interpolation strategies, using the input images of Figure 1. Structure transfer reduces ghosting, and clipped Laplacian blending (CLB) reduces blurring.*

5 Structure transfer

The coarse and fine images often come from different sources, so their detail structure generally does not align precisely. Consequently, any linear blending operation effectively creates a superposition of features from both images (Figure 6a,c).

To address this ghosting problem, our idea is to trust the detail from only one of the two images, namely the finer image. This choice is easily motivated. Imagery is typically captured at the limit of the acquisition resolution, and may therefore suffer from chromatic aberration, sensor noise, or demosaicing error. By combining many pixels of the finer image using a high-quality downsampling, we reduce these defects.

Therefore, the goal is to find a new coarse image x_c that combines (1) the structural detail of the downsampled fine image $D_f^c \hat{x}_f$ and (2) the local color distribution of the original coarse image $\hat{x}_c$. We refer to $S = D_f^c \hat{x}_f$ and $C = \hat{x}_c$ as the structure and color images, respectively.

Our solution, *structure transfer*, is to build a Gaussian model for the local distribution of colors in the neighborhood of each pixel in both images, and to use the z-score (also called the standard score) of the center pixel from S to select the color value with the identical score in C. Concretely, our algorithm performs the following steps at each pixel location (Figure 7):

- Compute the mean μ_S and standard deviation σ_S of the neighborhood in the structure image.
- Find $z = (v - \mu_S)/\sigma_S$ where v is the color of the center pixel.
- Obtain the new color as $v' = \mu_C + z\sigma_C$ where μ_C and σ_C are the neighborhood statistics in the color image.

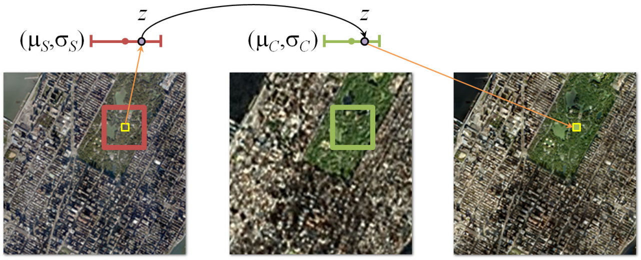

Structure image S

Color image C

Output

Figure 7: *Structure transfer. For each pixel in* S*, we compute its z-score within its weighted local window and output the equal-scored value from the corresponding window of* C.

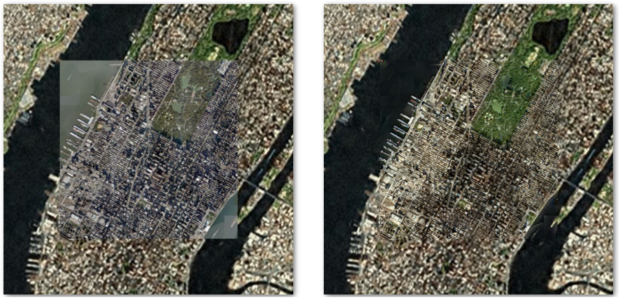

Simple downsampling

Structure transfer

Figure 8: *Unlike simple downsampling, structure transfer is able to preserve appearance continuity at the boundaries of sparsely defined data (here the inset square).*

This computation is performed separately for each color channel. We additionally weight the contributions of pixels in the window using a 2D Gaussian; we have obtained the best results with a standard deviation of 4 pixels over a window of 21^2 pixels.

Structure transfer approximates the maximization (2), as it preserves the local luminance (mean value μ) and contrast (σ) of the color image C while altering the detail (z-scores) to correlate with the structure image S. We illustrate this in Figure 9, where our result (c) has incorporated the structure and color from the respective inputs (a,b). The intermediate z-scores, visualized in Figure 9d, are quite different from a traditional high-pass linear filter or ratio image, in that the magnitudes adjust to the local contrast of the structure image. In the context of our full system, structure transfer reduces blurring (right column of Figure 6), and provides excellent appearance continuity at the boundary edges of sparsely defined fine-scale imagery (Figure 8).

Optimization Because the spatial Gaussian weighting used to compute the 21×21 window statistics (μ,σ) is separable, we efficiently amortize this computation over adjacent pixels. For each row of pixels, we first compute Gaussian-weighted vertical sums $\sum w_i v_i$ and $\sum w_i {v_i}^2$ in each 21×1 column centered about the row. Then for each pixel, we further combine these initial sums using 1D Gaussian weights over a 1×21 horizontal window. Finally we determine $\mu = \sum w_i v_i$ and $\sigma = \sqrt{\sum w_i {v_i}^2 - (\sum w_i v_i)^2}$.

Comparison to global color transfer As an alternative to our windowed z-score transfer, we also considered traditional global transfer methods (histogram transfer [Gonzalez and Woods 1992] and color transfer [Reinhard et al. 2001]). Applying these on a single image tile performs poorly as it does not allow local adaptation (Figure 9e; e.g., note how the river does not attain the expected appearance). As this problem is only exacerbated for larger images, a global approach is clearly inappropriate for our problem domain.

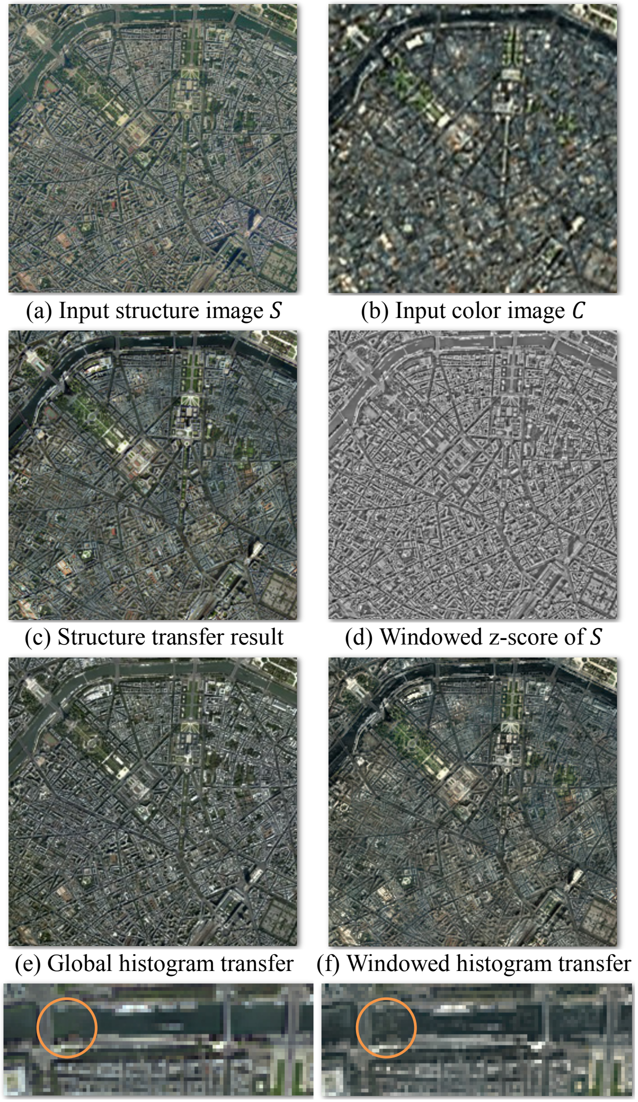

(a) Input structure image S (b) Input color image C

(c) Structure transfer result (d) Windowed z-score of S

(e) Global histogram transfer (f) Windowed histogram transfer

(g) Close-up of (c) (h) Close-up of (f)

Figure 9: *Structure transfer (c) gathers the structure and color from the respective input images (a,b) using a simple z-score construction. For illustration, we show (d) the z-score computed on the luminance channel. By comparison, global histogram transfer (e) lacks local adaptivity, and windowed histogram transfer (f) results in characteristic grain noise artifacts (h).*

We also attempted a windowed version of histogram transfer (Figure 9f), but found that this led to the same type of noise grain artifacts (Figure 9g) observed by Pitié et al. in their (global) histogram transfer work [2007]. In addition to producing higher-quality results (Figure 9h), our optimized z-score transfer algorithm allows much faster execution.

6 Pyramid construction

To create the intermediate images $\{x_l \mid c < l < f\}$, we minimize the pixel differences between successive levels. Our approach defines inter-level differences as the mean squared error (MSE) between the downsampled finer image and the coarser image:

$$\min_{x_{c+1}\dots x_{f-1}} \sum_{l=c..f-1} 4^{-l}\|D_{l+1}x_{l+1} - x_l\|^2. \tag{4}$$

Since this minimization defines a sparse linear system, we could solve it using an iterative solver. However, we will show that the global minimum of (4) can be directly approximated using a far more efficient algorithm.

6.1 Clipped Laplacian blending

As derived in the appendix, minimizing (4) results in the local inter-level constraint

$$D_l x_l = \tfrac{1}{2}\left(x_{l-1} + D_{l+1}^{l-1} x_{l+1}\right). \tag{5}$$

That is, the downsampling of each image should be a blended combination of the next-coarser image and the *twice*-downsampled next-finer image.

In concept, we can create a series of images that satisfies this constraint by directly building their Laplacian pyramids. The endpoints are given by the input coarse and fine images, x_c and x_f. The Laplacian pyramid of each intermediate image x_l can be found by first linearly blending the Laplacian pyramids of the inputs, *but only up to the level of the coarse image*, and then copying details from the fine image (Figure 10). Formally,

$$\mathcal{L}_k^{x_l} = \begin{cases} (1-\alpha_l)\mathcal{L}_k^{x_c} + \alpha_l \mathcal{L}_k^{x_f} & k \le c \\ \mathcal{L}_k^{x_f} & k > c, \end{cases} \tag{6}$$

where α_l is a simple interpolation weight, $\alpha_l = (l-c)/(f-c)$.

We refer to this scheme as *clipped Laplacian blending,* due to the intuitive Laplacian construction given above. However, a more efficient construction is possible; significantly, *it avoids having to compute and store Laplacian pyramids altogether.*

Efficient solution From the definition of a Laplacian pyramid, $x_l = \sum_{k=0\dots l} U_k^l \mathcal{L}_k^{x_l}$, we can rewrite (6) as

$$x_l = (1-\alpha_l)U_c^l d_c + \mathcal{G}_l^{x_f}, \text{ with } d_c = x_c - \mathcal{G}_c^{x_f}, \tag{7}$$

which is proven in the appendix to satisfy constraint (5). This interpretation leads to the construction illustrated in Figure 11.

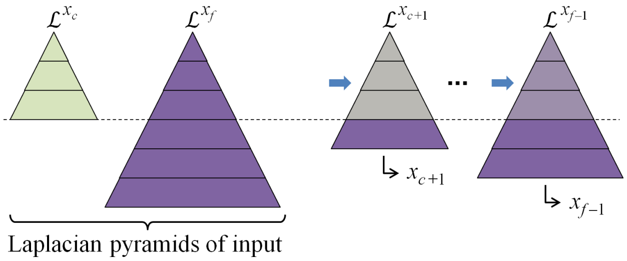

Figure 10: *Clipped Laplacian blending creates intermediate-resolution images by smoothly transitioning coarse levels of the Laplacian pyramids while iteratively adding intact fine detail.*

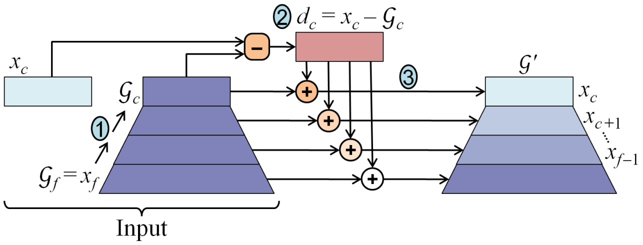

Figure 11: *Equivalent efficient blending algorithm with 3 simple steps: (1) downsampling to form Gaussian pyramid, (2) coarse-level differencing, and (3) fading the difference into the pyramid.*

We create the Gaussian pyramid $\mathcal{G}^{x_f}$ of the fine image x_f, compute the difference d_c between the coarse image and the fine image downsampled to level c, upsample that difference to the intermediate level, and fade it into the Gaussian pyramid. This solution offers a simple recurrence that lets all levels be evaluated in an efficient sequence of two passes over a pyramid structure. The complete algorithm is as follows:

```
$(x_{c+1} \dots x_{f-1}) \leftarrow$ ClippedLaplacianBlend$(x_c, x_f)$ {
  $\mathcal{G}_f = x_f$                          // Create the Gaussian pyramid of $x_f$
  for $l = f-1 \dots c$                   //  by successive fine-to-coarse
    $\mathcal{G}_l = D_{l+1}\mathcal{G}_{l+1}$               //  downsampling operations.
  $d = x_c - \mathcal{G}_c$                      // Compute the coarse difference.
  for $l = c+1 \dots f-1$                 // Traverse the Gaussian pyramid,
    $d = U_{l-1} d$                       //  upsampling the difference image,
    $\alpha_l = (l-c)/(f-c)$              //  and adding a faded fraction
    $x_l = \mathcal{G}_l + (1-\alpha_l) d$               //  of it at each level.
}
```

Comparison to linear interpolation One might consider an alternative form of the minimization (4), using $\|x_{l+1} - U_l x_l\|^2$ as the MSE metric—that is, defining inter-level differences using the upsampled coarse level rather than the downsampled fine level. In fact, this formulation corresponds exactly to standard linear interpolation, which we illustrate in the top row of Figure 6. As one might expect, direct linear interpolation results in ghosting artifacts; in comparison, clipped Laplacian blending (bottom row) yields much sharper results.

6.2 Error analysis for non-orthogonal filters

The algorithms developed in Section 6.1 (and the corresponding derivations in the appendix) assume that the up/downsampling filters used are orthogonal and transposes of each other. Formally,

$$D_l D_l^T = \tfrac{1}{4} I \quad \text{and} \quad D_l = U_{l-1}^T \, .$$

The only low-pass filter that exactly satisfies both assumptions is the box filter, which is undesirable due to poor frequency characteristics. We chose to use higher-order cubic filters for their better frequency response; however, since they are not strictly orthogonal they will introduce some small amount of error.

As an empirical evaluation, we compared results from figures in this paper against reference solutions obtained by directly minimizing (4) using Gauss-Seidel relaxation. This analysis uses the coarse image after structure transfer. Measuring the summed inter-level visual difference (4) for both sets of results, we find that the clipped Laplacian blending results typically differ by less than 1% from reference, with the greatest difference being under 3% (see Table 1). Subjectively, the results are visually indistinguishable.

Dataset	Clipped Laplacian blend	Reference solution	% Error
Figure 8	0.0034	0.0033	2.37%
Figure 12 row 1	0.0094	0.0093	1.38%
Figure 12 row 2	0.0106	0.0106	0.17%
Figure 12 row 3	0.0672	0.0671	0.18%
Figure 12 row 4	0.0130	0.0129	1.10%
Figure 12 row 5	0.0139	0.0138	0.41%
Figure 12 row 6	0.0092	0.0091	0.85%

Table 1: *Comparison of summed inter-level differences for the image pyramid created by clipped Laplacian blending and that obtained with the global linear least-squares solution.*

7 Implementation details

Because imagery can be quite large (e.g. potentially covering the Earth), it is typically partitioned into tiles, both for efficient processing and for fast delivery over the Internet. Fortunately, our two techniques (structure transfer and clipped Laplacian blending) only require access to local data. We exploit this locality to design a fast out-of-core processing algorithm.

We maintain images $\mathcal{G}_l$,x_l,d_l in 256^2 tiles, in correspondence with the input. We would like to minimize costly disk accesses, but in the course of processing a large image pyramid it becomes necessary to temporarily store some tiles to disk while new tiles are computed. To effectively manage this problem, we implemented a tile cache tailored to the access pattern of our algorithm.

Since we know ahead of time the tile access order of our algorithm, we can employ the optimal caching strategy, which is to evict the tile that will be needed furthest in the future [Belady 1966]. Furthermore, we use the tile access order to pre-cache tiles in a background thread. We tried a number of traversal schemes, and found that generating the finest-level tiles in Hilbert-curve order gave the best caching performance.

Our implementation processes 64 Gpixels in 18 hours on a dual-core Intel Core 2 PC. Because the technique is parallelizable, larger datasets could be processed on a compute cluster.

8 Additional results and discussion

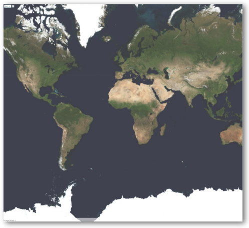

Our main dataset is imagery of the Earth's surface sampled over a regular grid under a Mercator projection. In the image pyramid, the coarsest resolution (level 0) contains a single 256^2 image tile, shown inset. Level 20 conceptually contains 2^{40} such tiles, but is defined quite sparsely. The input imagery comes from 3 main sources: level 8 (4-Gpixel) is "Blue Marble" satellite imagery; level 13 (4-Tpixel) is "Landsat" satellite imagery; and levels 14 and above contain sparsely defined aerial photography. Therefore, in most areas there are two discontinuous transitions across scales: from level 8 to 9, and from level 13 to 14.

We applied our scheme to improve both of these transitions. Finding the number of levels over which to perform the transition is content-dependent and somewhat subjective. As a general rule we strove to apply as short a transition as possible while still maintaining visual smoothness; ultimately we found that 4 transition levels was sufficient for transitions from Landsat to aerial photography. For the Blue Marble to Landsat transition, the color spaces were already well correlated and we were therefore able to generate good results using 3 levels.

The top three rows of Figure 12 show examples of Blue Marble to Landsat transition, and the next two rows show examples of Landsat to aerial transition. The structure-transferred results in the middle column show the benefit of injecting the additional detail from the fine-scale images. The left column shows that modifying the detail structure does not result in objectionable spatial seams in the case that the fine-scale content is only sparsely defined.

Animations The accompanying video shows 2×2 windows that compare zooming using different schemes: abrupt image transition, simple linear interpolation, CLB, and structure transfer plus CLB. The video also shows real-time zooming from space to ground level, with both the original image data and our results.

Limitations The third row of Figure 12 shows a difficult case where the coarse and fine images differ substantially due to the difference in ice coverage. In this case, gradual fading is unavoidable although still less disconcerting than abrupt transitions (see videos). The fourth row shows that if the source fine-scale image is poorly stitched (e.g. combines color and grayscale content), the seams are interpreted by the algorithm as structure and propagated to coarser levels; a reasonable solution in such cases would be to recolor the fine image as a preprocess. As shown in Figure 8, our method is resilient to slight misregistrations between source images. However, performing a non-rigid registration [Crum et al. 2004] beforehand may lead to more desirable results.

Quantitative analysis Table 2 reports the quality of results on the data in the last row of Figure 12, as measured by the two terms of our objective (the inter-level structural similarity MSSIM and the coarse-level luminance-contrast fidelity Mlc). The input data suffers from a discontinuous transition between levels 8 and 9. Clipped Laplacian blending improves results significantly, but ghosting adversely affects inter-level continuity. Introduction of structure transfer leads to an image pyramid with the best objective score. Table 3 summarizes these results across all the test images. The numbers confirm our observation that the new image pyramids are visually smoother.

Objective function E in (1)	Original abrupt transition	Linear blend	Clipped Laplacian blend	Structure transfer + CLB
MSSIM	6.991	7.616	7.796	7.959
level 4↔5	1.000	1.000	1.000	0.997
level 5↔6	1.000	1.000	1.000	1.000
level 6↔7	1.000	1.000	1.000	1.000
level 7↔8	1.000	1.000	1.000	1.000
level 8↔9	-0.009	0.906	0.913	0.983
level 9↔10	1.000	0.856	0.947	0.991
level 10↔11	1.000	0.883	0.962	0.994
level 11↔12	1.000	0.972	0.975	0.994
Mlc	5.000	5.000	5.000	4.915
level 4	1.000	1.000	1.000	1.000
level 5	1.000	1.000	1.000	0.996
level 6	1.000	1.000	1.000	0.965
level 7	1.000	1.000	1.000	0.968
level 8	1.000	1.000	1.000	0.986
E=MSSIM+Mlc	11.991	12.616	12.797	12.874

Table 2: *Quantitative results for the images in the last row of Figure 12.*

	Objective function E in (1)			
Dataset	Original abrupt transition	Linear blend	Clipped Laplacian blend	Structure transfer + CLB
Figure 9	12.197	12.700	12.851	12.874
Figure 12 row 1	12.134	12.660	12.812	12.875
Figure 12 row 2	12.404	12.719	12.816	12.839
Figure 12 row 3	12.011	12.211	12.412	12.448
Figure 12 row 4	12.077	12.639	12.819	12.882
Figure 12 row 5	11.960	12.513	12.762	12.916
Figure 12 row 6	11.991	12.616	12.797	12.874

Table 3: *Summary of quantitative results across all datasets.*

9 Summary and future work

We have presented two new techniques that enable fast creation of smooth visual pyramids from dissimilar imagery, and demonstrated practical results on large datasets with a variety of content.

As future work, one could consider more sophisticated Laplacian pyramid representations [e.g., Zarbman et al. 2008]. Structure transfer could be approached as a general optimization, much like the halftoning technique of Pang et al. [2008]. It would be interesting to exploit information from input images across multiple scales to aid in image stitching.

Structure transfer and clipped Laplacian blending are powerful tools that are likely to prove valuable in other application areas with aligned imagery. In particular, a number of recent works in computational photography have used registered images with different exposures, focal lengths, flash settings, aperture sizes, image sensors, etc. [Petschnigg et al. 2004; Krishnan and Fergus 2009]. One can also envision applications in embellishment of wide-angle panoramic photography with high-resolution overlays.

Acknowledgments

We would like to thank Matt Uyttendaele and Michael Kazhdan for discussions, Eric Stolnitz for providing a Deep Zoom sample application, Duncan Lawler and Nikolai Faaland for their help with the Virtual Earth 3D control, and NASA, NOAA, and USGS for the source imagery used in the experiments.

References

Agarwala, A., Dontcheva, M., Agrawala, M., Drucker, S., Colburn, A., Curless, B., Salesin, D., And Cohen, M. 2004. Interactive digital photomontage. *ACM Trans. on Graphics*, 23, 3.

Antonini, M., Barlaud, M., Mathieu, P., and Daubechies, I. 1992. Image coding using wavelet transform. *IEEE Trans. on Image processing*, 1, 2.

Belady, L. 1966. A study of replacement algorithms for a virtual-storage computer. *IBM Systems Journal*, 5, 2.

Burt, P., and Adelson, E. 1983. The Laplacian pyramid as a compact image code. *IEEE Trans. on Communications*, 31, 4.

Burt, P., and Adelson, E. 1983. A multiresolution spline with application to image mosaics, *ACM Trans. on Graphics*, 2, 4.

Chavez, P., Sides, S., and Anderson, J. 1991. Comparison of three different methods to merge multiresolution and multispectral data: Landsat TM and SPOT panchromatic. *Photogrammetric Engineering & Remote Sensing*, 57, 3.

Crum, W., Hartkens, T., and Hill, D. 2004. Non-rigid image registration: theory and practice. *British Journal of Radiology*.

Gonzalez, R., and Woods, R. 1992. *Digital Image Processing*. Addison Wesley.

Keys, R. 1981. Cubic convolution interpolation for digital image processing. *IEEE Trans. on Acoustics, Speech, and Signal Processing*, 29, 6.

Kopf, J., Cohen, M., Lischinski, D., And Uyttendaele, M. 2007. Joint bilateral upsampling. *ACM Trans. on Graphics*, 26, 3.

Krishnan, D., and Fergus, R. 2009. Dark flash photography. *ACM Trans. on Graphics*, 28, 3.

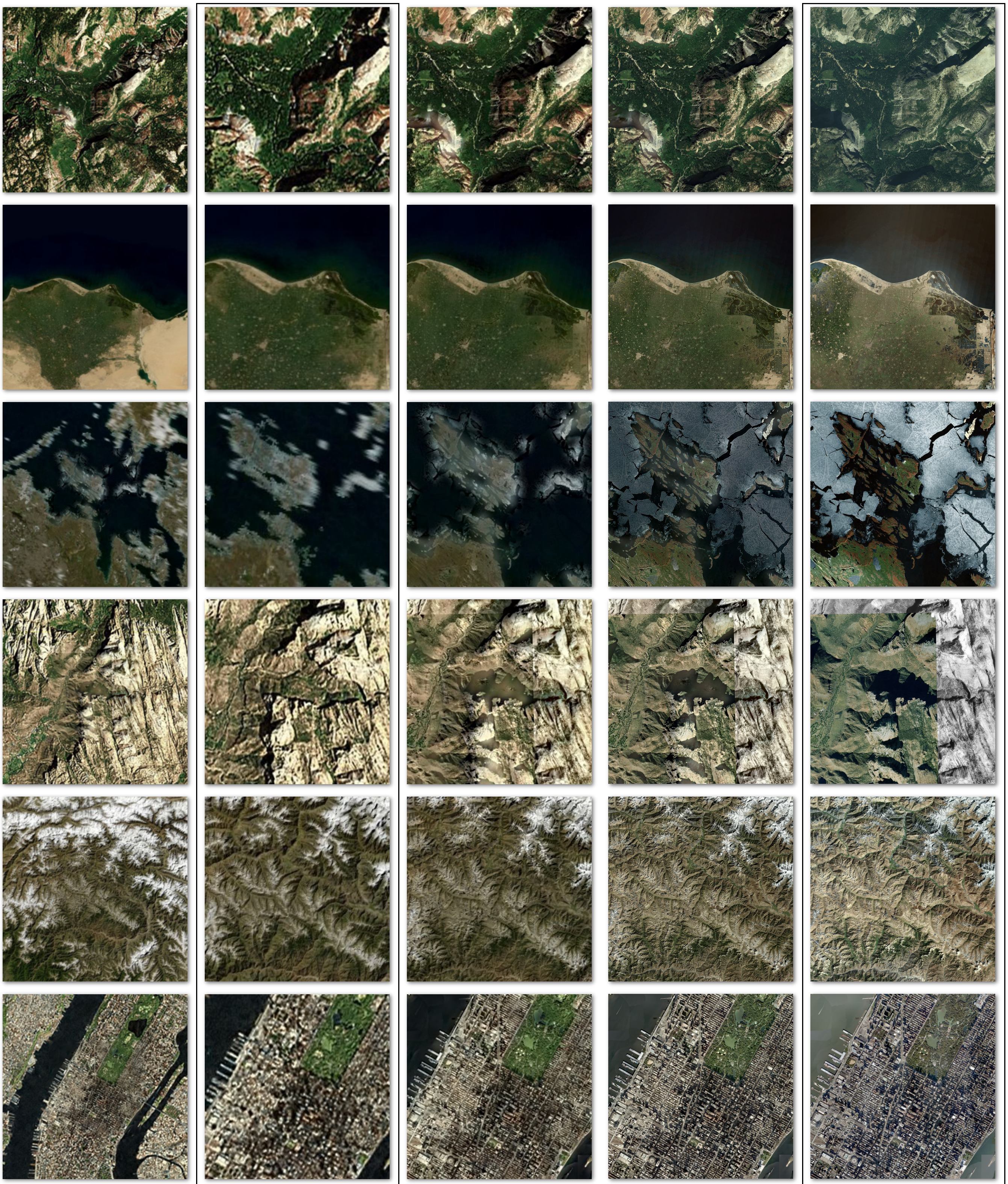

(a) Result at coarser level

(b) Input coarse image (256^2 resolution)

(c) Structure transfer (256^2)

(d) Blended interm. level (1024^2)

(e) Input fine image (4096^2 resolution)

Figure 12: *Collection of results. In each row, the inputs are (b) a 256^2 coarse image, and (e) a 4096^2 fine image. Column (c) shows the result of structure transfer (a new 256^2 image), and column (d) shows clipped Laplacian blending at the intermediate level with 1024^2 resolution. The view of the next-coarser level in column (a) demonstrates the spatial continuity with respect to the surrounding content.*

LIU, Z., SHAN, Y., AND ZHANG, Z. 2001. Expressive expression mapping with ratio images. *ACM SIGGRAPH Proceedings*.

MITCHELL, D., AND NETRAVALI, A. 1988. Reconstruction filters in computer graphics. *ACM SIGGRAPH Proceedings*.

OLIVA, A., TORRALBA, A., AND SCHYNS, P. 2006. Hybrid images. *ACM Trans. on Graphics*, 25, 3.

PANG, W.-M., QU, Y., WONG, T.-T., COHEN-OR, D., AND HENG, P.-A. 2008. Structure-aware halftoning. *ACM Trans. on Graphics*, 27, 3.

PÉREZ, P., GANGNET, M., AND BLAKE, A. 2003. Poisson image editing. *ACM Trans. on Graphics*, 22, 3.

PETSCHNIGG, G., AGRAWALA, M., HOPPE, H., SZELISKI, R., COHEN, M., TOYAMA, K. 2004. Digital photography with flash and no-flash image pairs. *ACM Trans. on Graphics*, 23, 3.

PITIÉ, F., KOKARAM, A., AND DAHYOT, R. 2007. Automated color grading using color distribution transfer. *Computer Vision and Image Understanding*, 107, 1–2.

PIZER, S., AMBURN, E., AUSTIN, J., CROMARTIE, R., GESELOWITZ, A., GREER, T., ROMENY, B., ZIMMERMAN, J., AND ZUIDERVELD, K. 1987. Adaptive histogram equalization and its variations. *Computer Vision, Graphics, and Image Processing*, 39.

POHL, C., AND VAN GENDEREN, J.L. 1998. Multisensor image fusion in remote sensing: concepts, methods and applications. *Int. J. Remote Sensing*, 19, 5.

REINHARD, E., ASHIKHMIN, M., GOOCH, B, AND SHIRLEY, P. 2001. Color transfer between images. *IEEE CG&A*, 21, 5.

STATHAKI, T. 2008. *Image Fusion: Algorithms and Applications*. Academic Press.

SZELISKI, R. 2006. Image alignment and stitching: A tutorial. *Foundations and Trends in Comp. Graphics and Vision*, 2(1).

WANG, Z., BOVIK, A., SHEIKH, H., AND SIMONCELLI, E. 2004. Image quality assessment: From error visibility to structural similarity. *IEEE Trans. on Image Processing*, 13, 4.

WILLIAMS, L. 1983. Pyramidal parametrics. *ACM SIGGRAPH Proceedings*.

WITKIN, A. 1983. Scale-space filtering: A new approach to multi-scale description. *Proc. 8th Int. Joint Conf. Art. Intell.*

ZARBMAN, Z., FATTAL, R., LISCHINSKI, D., AND SZELISKI, R. 2008. Edge-preserving decompositions for multi-scale tone and detail manipulation. *ACM Trans. on Graphics*, 27, 3.

Appendix: Detailed proofs and derivations

Minimizing (4) results in inter-level constraint (5)

Taking the partial derivative of (4) with respect to a level x_l and setting it to zero, we obtain

$$\begin{aligned} 2\left(4^{-(l-1)}\right)D_l^T(D_l x_l - x_{l-1}) - 2(4^{-l})(D_{l+1}x_{l+1} - x_l) &= \\ 4D_l D_l^T(D_l x_l - x_{l-1}) - D_l(D_{l+1}x_{l+1} - x_l) &= 0. \end{aligned}$$

Using the assumption $D_l D_l^T = \frac{1}{4}I$, we obtain

$$\begin{aligned} &(D_l x_l - x_{l-1}) - \left(D_{l+1}^{l-1}x_{l+1} - D_l x_l\right) = 0 \\ \Rightarrow\quad &(D_l + D_l)x_l = x_{l-1} + D_{l+1}^{l-1}x_{l+1} \\ \Rightarrow\quad &D_l x_l = \tfrac{1}{2}\left(x_{l-1} + D_{l+1}^{l-1}x_{l+1}\right). \end{aligned}$$

Efficient solution (7) satisfies constraint (5)

For $c < l < f$, we must show that

$$\begin{aligned} &D_l\left((1-\alpha_l)U_c^l d_c + \mathcal{G}_l^{x_f}\right) \\ &\qquad = \tfrac{1}{2}\begin{pmatrix} \left((1-\alpha_{l-1})U_c^{l-1}d_c + \mathcal{G}_{l-1}^{x_f}\right) + \\ D_{l+1}^{l-1}\left((1-\alpha_{l+1})U_c^{l+1}d_c + \mathcal{G}_{l+1}^{x_f}\right) \end{pmatrix}. \end{aligned}$$

Assuming $D_l U_{l-1} = I$, we obtain

$$(1-\alpha_l)U_c^{l-1}d_c + \mathcal{G}_{l-1}^{x_f} = \tfrac{1}{2}\begin{pmatrix} (1-\alpha_{l-1})U_c^{l-1}d_c + \mathcal{G}_{l-1}^{x_f} + \\ (1-\alpha_{l+1})U_c^{l-1}d_c + \mathcal{G}_{l-1}^{x_f} \end{pmatrix}$$

$$\Rightarrow\quad U_c^{l-1}d_c\left((1-\alpha_l) - \tfrac{1}{2}(1-\alpha_{l-1}) - \tfrac{1}{2}(1-\alpha_{l+1})\right) = 0.$$

The above holds true if

$$\alpha_l = \tfrac{1}{2}(\alpha_{l-1} + \alpha_{l+1}),$$

which is satisfied by the linear interpolation weight $\alpha_l = \frac{l-c}{f-c}$.

For $l = c$, we have $\alpha_c = 0$, and can therefore verify that

$$(1-\alpha_c)U_c^c d_c + \mathcal{G}_c^{x_f} = \left(x_c - \mathcal{G}_c^{x_f}\right) + \mathcal{G}_c^{x_f} = x_c.$$

For $l = f$, we have $\alpha_f = 1$, and can therefore verify that

$$\left(1-\alpha_f\right)U_c^f d_c + \mathcal{G}_f^{x_f} = \mathcal{G}_f^{x_f} = x_f.$$

Derivation of efficient solution (7) from CLB (6)

Using the definition of a Laplacian pyramid,

$$\begin{aligned} x_l &= U_{l-1}\left(\cdots\left(U_0\left(\mathcal{L}_0^{x_l}\right) + \mathcal{L}_1^{x_l}\right) + \cdots\right) + \mathcal{L}_l^{x_l} \\ &= \sum_{k=0\ldots l} U_k^l \mathcal{L}_k^{x_l}, \end{aligned}$$

the solution given by the Clipped Laplacian blending (6),

$$\mathcal{L}_k^{x_l} = \begin{cases} (1-\alpha_l)\mathcal{L}_k^{x_c} + \alpha_l\mathcal{L}_k^{x_f} & k \le c \\ \mathcal{L}_k^{x_f} & k > c, \end{cases}$$

is re-expressed as the efficient solution (7) as follows:

$$\begin{aligned} x_l &= \sum_{k=0\ldots c} U_k^l\left((1-\alpha_l)\mathcal{L}_k^{x_c} + \alpha_l\mathcal{L}_k^{x_f}\right) + \sum_{k=c+1\ldots l} U_k^l\mathcal{L}_k^{x_f} \\ &= U_c^l\left((1-\alpha_l)\sum_{k=0\ldots c} U_k^c\mathcal{L}_k^{x_c} + \alpha_l\sum_{k=0\ldots c} U_k^c\mathcal{L}_k^{x_f}\right) \\ &\qquad + \sum_{k=c+1\ldots l} U_k^l\mathcal{L}_k^{x_f} \\ &= U_c^l\left((1-\alpha_l)x_c + \alpha_l\mathcal{G}_c^{x_f}\right) + \sum_{k=c+1\ldots l} U_k^l\mathcal{L}_k^{x_f} \\ &= U_c^l(1-\alpha_l)\left(x_c - \mathcal{G}_c^{x_f}\right) + U_c^l\mathcal{G}_c^{x_f} + \sum_{k=c+1\ldots l} U_k^l\mathcal{L}_k^{x_f} \\ &= (1-\alpha_l)U_c^l d_c + \mathcal{G}_l^{x_f} \quad\text{with}\quad d_c = x_c - \mathcal{G}_c^{x_f}. \end{aligned}$$